LAWRENCE
LIVERMORE
NATIONAL
LABORATORY

LLNL-BOOK-405555

Application of Electron Backscatter Diffraction to Phase Identification

B. S. El-Dasher, A. Deal

July 22, 2008

Electron Backscatter Diffraction in Materials Science, 2nd Edition

Disclaimer

Application of Electron Backscatter Diffraction to Phase Identification

Bassem El-Dasher[1] and Andrew Deal[2]

[1]Lawrence Livermore National Laboratory, Livermore, CA 94550 USA

[2]GE Global Research, Niskayuna, NY, 12309 USA

Abstract

The identification of crystalline phases in solids requires knowledge of two microstructural properties: crystallographic structure and chemical composition. Traditionally, this has been accomplished using X-ray diffraction techniques where the measured crystallographic information, in combination with separate chemical composition measurements for specimens of unknown pedigrees, is used to deduce the unknown phases. With the latest microstructural analysis tools for scanning electron microscopes, both the crystallography and composition can be determined in a single analysis utilizing electron backscatter diffraction and energy dispersive spectroscopy, respectively. In this chapter, we discuss the approach required to perform these experiments, elucidate the benefits and limitations of this technique, and detail via case studies how composition, crystallography, and diffraction contrast can be used as phase discriminators.

Introduction

The distribution, morphology, and stability of material phases govern the bulk properties of virtually all of the technologically relevant materials used to design engineering components and products. Phase identification and characterization are therefore critical to the use and development of practical materials. In this chapter, we will focus on the application of Electron Backscatter Diffraction (EBSD) to phase identification.

Complete phase identification must include two components that identify the phase uniquely: structure and chemistry. Strictly speaking, unambiguous crystalline phase identification requires determining the exact periodic, atomic arrangement of the unknown phase. This is the information contained in the space group, lattice parameters, and the chemical occupancies of the space group's atomic positions for a given phase. Given its diffraction-based origins, the EBSD technique can directly satisfy the structural determination component of phase identification, but not without limitations. The complete data set of structural information contained within an EBSD pattern is difficult to extract, typically requiring non-standard setups and/or detectors, and space group and lattice parameter determination by EBSD has only been accomplished with meticulous manual scrutiny of the EBSD diffraction patterns (Baba-Kishi and Dingley 1989, Baba-Kishi and Dingley 1989a, Baba-Kishi 1998, Michael and Eades, 2000).

For comprehensive phase identification, EBSD needs to be supplemented with quantitative chemical characterization. Techniques such as energy or wavelength dispersive X-ray spectroscopy (EDS or WDS) are perfect complements to EBSD, as they also require a scanning electron microscope (SEM), allowing for simultaneous diffraction and compositional data collection. When the material pedigree is known however, this is not necessary, and successful phase differentiation and verification using semi-automated EBSD was demonstrated over a decade ago (Goehner and Michael 1996).

Despite its limitations, there are clear advantages of using EBSD for phase determination. These include spatial resolution, sample requirements, and the convenience/availability of other SEM techniques for phases analysis. EBSD lateral spatial resolution, 0.1μm-0.01μm depending the SEM, is approximately two orders of magnitude higher than conventional (non-synchrotron) X-ray diffraction (XRD) methods and two orders of magnitude lower than TEM, filling the gap between both techniques. Recently available commercial systems capable of processing over two hundred patterns per second have also allowed for EBSD datasets spanning tens of millimeters, effectively sampling an amount of material as statistically relevant as that sampled with XRD. Furthermore, EBSD is a bulk technique, and the meticulous preparation such as that required for electron-transparent thin specimens for TEM is unnecessary. SEM imaging can also provide morphological information to support an EBSD analysis, and SEMs equipped with EDS or WDS can assess the chemistry of the phase without additional sample preparation or transfer to another instrument. Combining all these capabilities with the statistical nature of EBSD also permits the study of previously inaccessible aspects of multi-phase materials such as simultaneous phase distribution, volume fraction, and orientation relationships. While these are advantages over the "traditional" XRD and TEM analyses, this does not imply that EBSD is the preferred alternative to either TEM or XRD, and in many cases, phase identification benefits greatly from the parallel use of these methods.

For a comprehensive review of EBSD's application to studying phase transformation, complete with over 600 references, the reader is directed to a recently compiled review by Gourgues-Lorenzon (Gourgues-Lorenzon 2007).

CONSIDERATIONS

There are multiple approaches to using EBSD to assist with phase identification, and these are typically dictated by the specific application. Nevertheless, there are some fundamental considerations

that equally apply regardless of approach, including: the use of prior sample knowledge and chemical information, basic manual scrutiny of patterns, and semi-automated database searching to identify an unknown phase. Before we address these, it is important to stress that two experimental requirements are essential to any attempt at phase identification using EBSD, regardless of the approach:

1. Accurate and precise geometric calibration
2. Obtaining the highest quality EBSD patterns

As discussed in other chapters (eds, insert chapter numbers here), the calibration of an EBSD system is highly sensitive to sample positioning and especially the sample-to-detector distance. Thus, the possibility of using a fixed set of calibration parameters (e.g. those established upon installation) for multiple samples is severely hindered by the tolerances of these measurements. For example, EBSD cameras are necessarily retractable, leading to slight inconsistencies in camera placement upon reinsertion, and sample positioning is even less repeatable. In modern SEMs, reported working distances are typically calculations based on ideal alignments and conditions, and they are often rounded to the nearest millimeter. These values are therefore not as precise as needed for placing a sample at precisely the same working distance, as required for EBSD phase identification. Changing the beam conditions on an instrument and refocusing can also result in a slightly different reported working distance (e.g. 0.1 mm or so for those that report this precision), even after degaussing. While this is not an issue for most SEM analyses, it is too imprecise for EBSD phase identification, and changes in sample and/or detector positions will affect all subsequent measurements, manual or automated, for phase identification. It is therefore absolutely critical to confirm or refine the calibration of the EBSD system *for each phase analysis performed*, either with a known, strain-free crystal phase in the sample or with a standard material such as copper or silicon.

Obtaining the highest possibly quality EBSD patterns from the phase of interest is just as critical. Typically, this is accomplished by using the CCD camera in its non-binned state to maximize the angular resolution of the pattern, although pixel binning may be necessary if sufficient signal is unobtainable. The quality of flat-fielding

(background subtraction) is also important, so care must be taken to ensure that static backgrounds acquired for the procedure are sufficiently free of crystallographic information and representative of the intensity distribution for the region examined. It is also helpful for most analyses to shorten the detector distance to maximize the pattern's angular range and expose as many of the major symmetry elements of the phase as possible. This is particularly valuable for lower symmetry phases and semi-automated EBSD phase identification. Both make use of well-separated Kikuchi bands to determine symmetry.

Generally speaking, an analysis of a completely unknown crystalline sample is a rare event. More often than not, a reasonable amount of prior knowledge will be available to the investigator. This may include the sample's origin, bulk chemistry, thermo-mechanical history, or even a list of expected phases and morphologies. In many cases, samples are often analyzed in a comparative set such that much of this information can be deduced from a more well-characterized and known variation. Prior sample knowledge should be used to thin down the list of phase possibilities. For example, commercial engineering materials such as steels, nickel-based superalloys, and titanium-based alloys have been heavily characterized over decades. Consequently, lists of expected phases, morphologies, chemistries, and occurrences can and should be extracted from literature and other sources for comparison with an unknown sample. This information should be consistent with any EBSD results for the phases in question. If the result of a phase identification experiment does not match what is expected based on prior sample knowledge, the analysis must be scrutinized for possible sources of error. If no sources of error are found, then the existence of the unexpected phase(s) should be weighed against any other outstanding aspects of the sample, such as material properties, for validation. In this way prior sample knowledge can increase the accuracy of an EBSD phase identification analysis. It is therefore extremely important for analysts to collect as much information about the sample prior to the EBSD analysis. This includes imaging the sample at several magnifications to identify the morphology and distribution of phases.

Understanding the chemistry of the phase of interest (and of the bulk sample if unknown) is an important in this approach. Qualitative chemical information can usually be accomplished with EDS. EDS is well-suited to supplement an EBSD phase identification since many modern SEMs are set up for simultaneous acquisition. An initial list of elements present in a phase can be generated with relative ease and reasonable accuracy. A full quantitative analysis is also possible if standards are available and the elemental x-ray peaks are well-separated in energy. However, it is important to realize when EDS is inadequate, and the substantially better energy resolution of WDS may be necessary to distinguish between elements with x-ray peaks close in energy. Similarly, the finer spatial resolution of Auger may be required if the phase size is significantly smaller than one micron. The phase chemistry information obtained with these techniques can often help narrow the field of possible phases. Caution should be used, however, with this approach. Phases in databases are typically reported with a specific stoichiometric composition, with no information about the solubility of other elements. As a simple example, alpha titanium (6/mmm) has a large solubility for aluminum, which will be detected in an EDS analysis of alpha in a Ti alloy. A database will typically list the alpha phase chemistry as pure Ti. Thus, a database search on phases containing both Ti and Al will not necessarily yield the alpha phase. As can be imagined, this problem is compounded for multi-element alloys containing phases with unknown solubility. In these cases, it is often better to investigate the structure before assessing the chemistry.

EBSD patterns contain a wealth of structural information, and manual scrutiny is a good starting point. A detailed review of manual pattern inspection and structure identification is available in the literature (Baba-Kishi 2002). Symmetry elements such as the mirror plane, 2-fold, 3-fold, 4-fold, and 6-fold axes of patterns in Fig. 1, may be identified in quality patterns. The presence or absence of symmetry elements can be used to narrow down the structure possibilities. For example, a 6-fold axis indicates that the crystal structure is hexagonal, and means that the number of possible point groups reduces from 32 to 7. On the other hand, it is helpful to acquire multiple EBSD patterns covering a significant amount of Kikuchi space ensure that a given

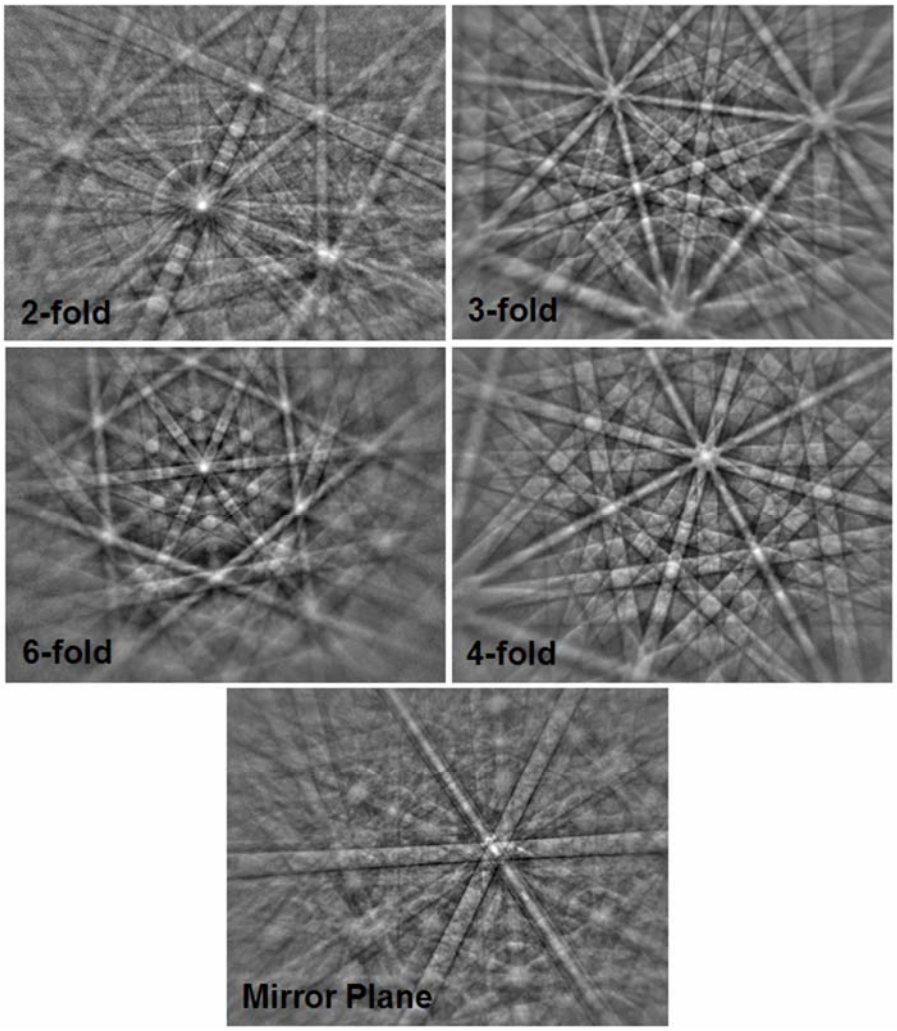

Figure 1. Diffraction patterns of the various symmetry elements that can be used to identify phases.

symmetry element is truly absent. This can be difficult for phases that have a preferential orientation in a single sample (e.g. castings, extrusions), and it may be necessary to analyze orthogonal cross-sections of the material and/or capture EBSD patterns at various stage tilts/rotations to bring different orientations into view. For semi-

automated EBSD analysis, identifying the bands in the patterns is vital to the subsequent computer analysis. While manual analysis provides the highest ultimate accuracy (by virtue of providing the most control), automated band-detection is of great benefit if large numbers of diffraction patterns are to be analyzed. In such cases, the resolution of the Hough transform should be maximized to correctly identify the band positions.

Once the bands in a high-quality, well-calibrated pattern are identified, automated phase matching can be performed using a phase database. This method is similar to the automated indexing of a single phase, except that the best solutions for multiple phases are compared against each other to find the best identification. Available databases can have thousands of entries, and it is impractical to compare all entries to the unknown phase even with modern computing power. Consequently, information obtained from prior sample knowledge, morphology, chemistry, and manual scrutiny of the pattern are critical to reduce the list of phase possibilities in the search, and a typical refinement reduces the scope of consideration to a few hundred phases or less. Evidence for correct phase identification should not be limited to a database match on a single EBSD pattern. Different patterns from the same phase should be compared and produce the same result (be self-consistent), and the identified phase should also be consistent with all the parameters used to refine the search. It should be noted that new phases are constantly discovered, and it is important to supplement a database with any recent phases from the literature that might be present in the unknown sample.

CASE STUDIES

In this section we present three case studies that are meant to guide the reader through approaches used to solve phase discrimination problems using EBSD. While not representative of all the experiments possible, these case studies are intended to represent typical applications of EBSD phase identification. The first of these shows how

compositional differences can be used to discriminate between phases using simultaneous EBSD and EDS acquisition. The second discusses the difficulties in differentiating structurally-similar phases on a size scale that is not amenable to simultaneous EBSD/EDS. Finally, the third shows how crystallographic discrimination can be used to yield quantitative statistical results.

We chose a Ni-based superalloy for each case study for several reasons. Ni-based superalloys are a class of engineering materials that have been developed over decades. The unique ability of these materials to maintain desirable properties at temperatures close to their melting temperatures allow them to be used for gas turbine components for power generation and aircraft. The integrity of these alloys at operating temperatures depends on the distribution and interaction of multiple phases. Consequently, accurate phase identification and characterization are vital to the success and quality control of these materials. Many of these phases are difficult to distinguish from each other based upon structure alone, necessitating the use of complementary analyses to correctly identify the phases.

Case 1: Simultaneous EBSD/EDS Phase Discrimination

There are several precipitates in superalloys that are difficult to distinguish by EBSD alone. Among these are relatively large, undesirable M(C,N) carbonitride inclusions that form during solidification. These phases are very stable and are difficult to dissolve in subsequent thermo-mechanical processing. Because of their cubic symmetry they are often confused with the matrix phase during automated EBSD analyses. However, their distinctly different chemistries make phase discrimination possible with simultaneous EDS acquisition and subsequent post-processing.

A sample of the Ni-based superalloy INCONEL 718 was chosen to demonstrate EBSD/EDS phase discrimination. The sample was metallographically prepared, and subsequent analyses were performed

with a Hitachi SU-70 thermal FEG SEM equipped with Oxford INCA X-Act EDS and HKL EBSD. Initial screening of potential phases was accomplished with backscattered electron imaging. Four potentially different phases were identified based on morphology and backscattered electron contrast: the large-grained matrix phase(s); a small elongated light grey phase that was homogeneously dispersed; a large, dark, blocky phase; and a bright, globular phase. Based on the phase morphology and metallurgical knowledge of the alloy these were expected to be the γ matrix, Nb-rich δ precipitates, and Ti or Nb-rich M(C,N) carbonitrdes, respectively. γ'', a nm scale phase structurally similar to the matrix, was not expected to be discernable in the SEM even if present in the alloy.

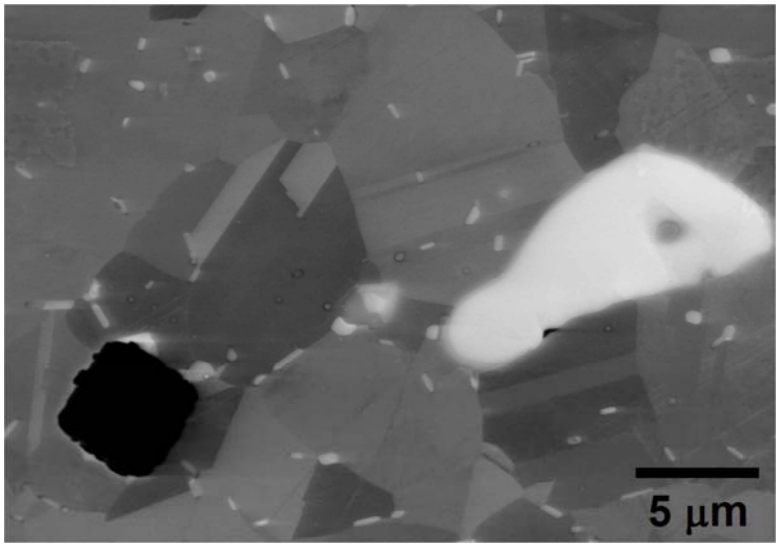

Figure 2. Backscattered electron image of the region of interest.

A region where all four distinguishable phases existed was chosen for analysis, shown in Fig. 2. After careful calibration, unbinned patterns from these phases were taken, as presented in Fig. 3. Crystallographic parameters of the four suspected phases, γ-Ni, δ–Ni_3Nb, TiN and NbC, were taken from the ICSD database. TiN and NbC are representative chemistries of the phases, since TiN has solubility for Nb and C and

NbC has solubility for Ti and N. The lattice parameters of all three cubic phases did not vary much, ranging from 0.356 to 0.447 nm. Kinematic simulations produced reflector lists for each phase, and the cubic phases had the same strong reflectors with only subtle intensity differences. The strong Kikuchi bands in each pattern were then manually detected. Subsequent automated phase matching with commercial software identified the elongated phase as δ unambiguously. However, differentiation between the other three phases was not conclusive. These phases were all identified as cubic by the software, but indexing between γ, TiN, and NbC was not consistent with the backscattered differentiation of the phases.

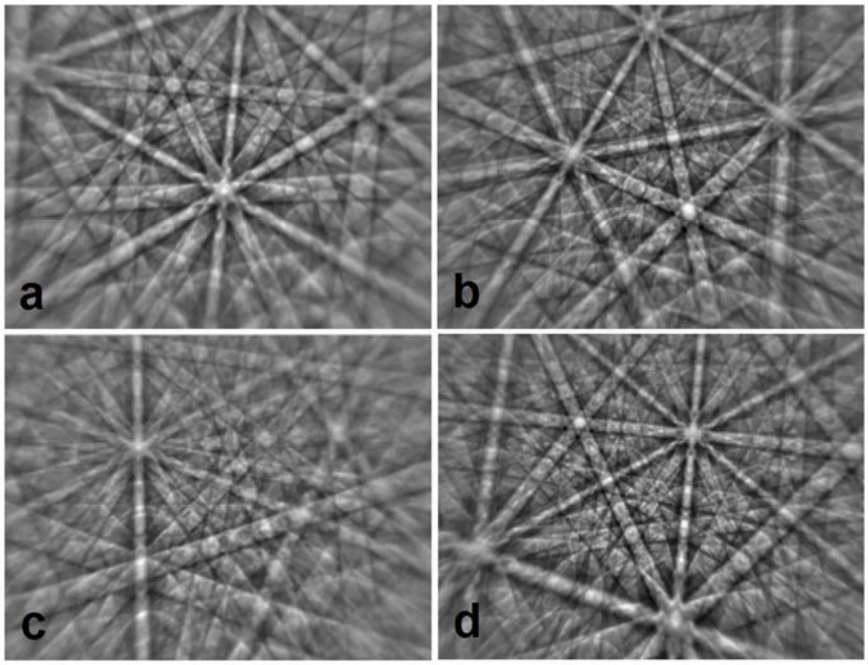

Figure 3. EBSD patterns of four apparent phases in Fig. 2 a) matrix grain b) dark , blocky phase c) small, elongated phase d) bright, globular phase

To distinguish between the cubic phases in the material, simultaneous EBSD/EDS acquisition was employed while mapping the region of interest with a 15kV electron beam. The microscope settings were adjusted to obtain a full spectrum x-ray count rate of 35,000 counts per second with a 28% dead time. EBSD indexing speed was slowed to approximately 9 points per second to ensure the collection of good x-ray statistics at each point. The step size for the map was 35nm over a 914x628 grid. Additionally, since the cubic phases could not be distinguished well structurally, only the γ and δ phases were included for automated differentiation during mapping.

The resulting phase map, together with the Ni, Nb, and Ti elemental maps, are shown in Fig. 4a. The EBSD indexing rate was 97% with only minor misindexing at the grain boundaries. These artifacts (less than 1% of the points) were removed upon initial post-processing. The γ and δ phases were readily distinguished by the automated phase differentiation, and the high Nb content in the δ phase areas supported the identification of that phase. However, it was very apparent from the EDS maps of Ni, Ti, and Nb that the blocky and globular phases had different chemistry than the matrix. Higher levels of carbon were also detected in these regions. Nitrogen could not be mapped with any accuracy due to an energy overlap with Ti. However, the morphology, detected chemistry, and cubic structure of the globular and blocky phases was consistent with M(C,N) carbonitrides.

By selective thresholding of the EDS maps and Boolean operations it was possible to automatically reassign regions of appropriate chemistry to either the TiN or NbC phases with post-processing software. The result is shown in Fig. 4b, which is a substantial improvement over phase differentiation by structure alone. A final piece of supporting evidence for the phase assignments was collected when the mapped region was examined optically. Cubic nitrides in Ni-based superalloys are recognizably yellow to orange in color as seen with a light microscope. Similarly, cubic carbides are often grey to lavender (Davis 1997), and the optical image of the region of interest, also shown in Fig. 4b, is consistent with the phases identified

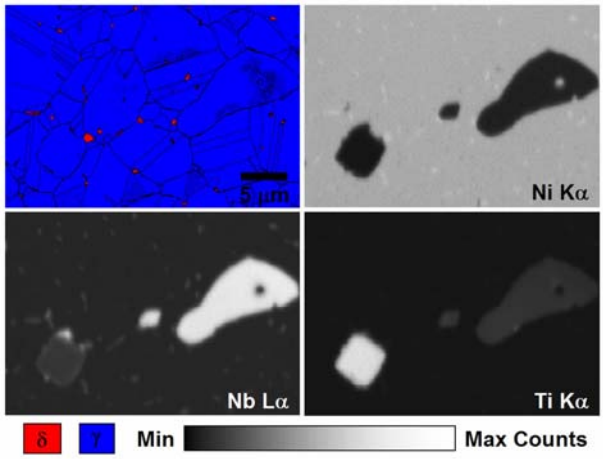

Figure 4a. EBSD and EDS maps of the region of interest (shown in Fig. 2) illustrating the initial resultant phase map, as well as the EDS signal from the Ni Kα, Nb Lα, and Ti Kα peaks.

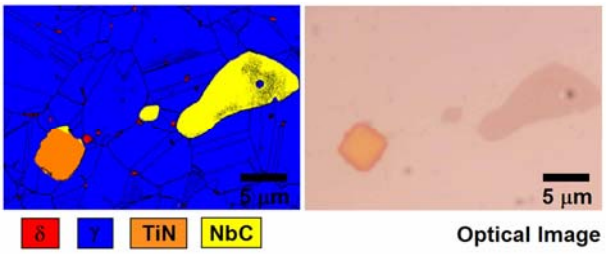

Figure 4b. The phase map obtained after incorporating the EDS information is shown in (4a). Assigned phases are corroborated by the colors observed in optical microscope image.

Case 2: Gamma and Gamma Prime

Two phases that are difficult to differentiate structurally with EBSD in many Ni-based superalloys are γ and γ'. The γ' phase, $Ni_3(Ti,Al)$, is an ordered precipitate that forms coherently from the γ matrix upon the

segregation of Ti and Al. Both γ and γ' phases have cubic crystal structures with lattice parameters that differ by no more than 0.5% in most commercial alloys. This small coherency strain, along with differences in elastic moduli and atomic ordering between the phases, is a major contributor to the strength of the material.

A sample of commercially available Rene' 88 bar stock was used to test the ability of conventional EBSD to accurately distinguish between γ and γ' under high resolution SEM conditions. The sample was heat treated to produce globular/blocky sub-micron γ' in a γ matrix. It was

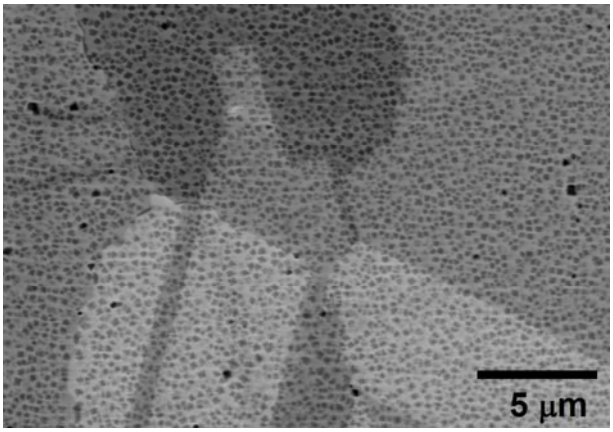

Figure 5. Backscattered electron micrograph revealing the γ' distribution within the γ matrix.

then metallographically prepared for EBSD. Subsequent analyses were performed with the same instrumentation used in the previous case study. Backscattered electron imaging, relying on chemical differences to provide phase contrast, revealed the distribution of γ' shown in Fig. 5.

After careful calibration, several pairs of non-binned EBSD patterns were taken from opposite sides of phase boundaries in parent γ grains. Over 30 frames were averaged for each pattern to reduce noise. A representative pair of patterns is presented in Fig. 6a. The sister patterns in the figure appear almost identical to the eye. However, subtle differences between the patterns do exist. Fig. 6b is a plot of the

contrast in the {200} Kikuchi band of both patterns, demonstrating that the band contrast is slightly stronger for the γ phase than for the γ'.

As a first attempt at differentiation, the γ and γ' phases were kinematically simulated to establish a reflector list for each phase. There were no appreciable differences in the generated reflector lists, but the γ phase had slightly larger calculated reflector intensities. From these lists, the number of reflectors was refined to represent the bands present in the patterns, and the position of the bands were detected

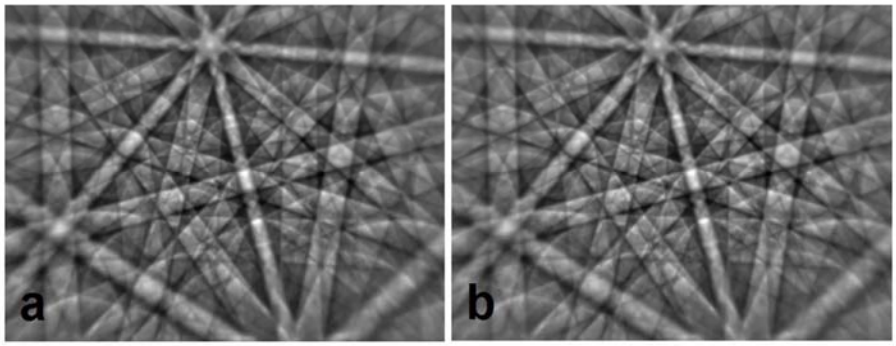

Figure 6a. EBSD patterns from (a) γ and (b) γ' appear virtually identical.

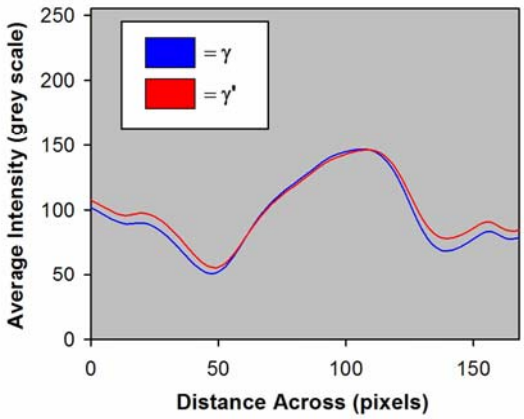

Figure 6b. A plot of the average grayscale value across the {200} bands in Fig. 6a demonstrating the contrast differences between γ and γ'.

manually for a pair of patterns. Subsequent computer indexing using commercial software could not distinguish between the patterns with any certainty, which was not surprising considering the structural similarities of the two phases.

Automated EBSD indexing and simultaneous EDS acquisition with a 15kV beam was attempted next. However, even by acquiring over 30,000 counts per second and 500ms of dwell time per pixel the phases

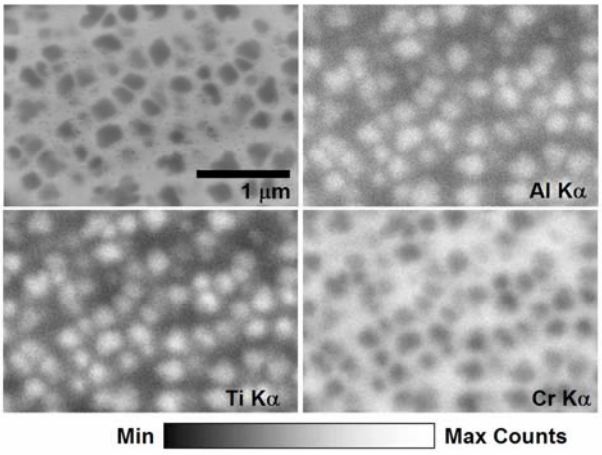

Figure 7. Backscattered electron image of the region mapped using EDS (top-left) and the associated distributions of Al, Ti, and Cr.

could not be distinguished from each other. While orientation was easily determined during EBSD mapping, the EDS maps did not show Ni, Ti, or Al segregation above the noise level. This was in part due to the fact that the size of the γ' approached the resolution of the EDS technique, which is generally on the order of a micron for standard analysis conditions. Detecting statistically significant segregation at a sub-micron level in this sample with EDS required an enormous number of x-ray counts. Fig. 7 shows a successful EDS map taken at 0^o tilt without simultaneous EBSD acquisition. The full-spectrum map was acquired continuously over 40 hours and consisted of well over 2 million frames. Stability of the region of interest was maintained with

the aid of a stage locking mechanism and drift correction software. While possible in principle to acquire an EBSD map at the same time and obtain phase differentiation, in practice several difficulties prevented such a measurement. At the tilts required for EBSD, sample drift becomes more of a problem, especially with drift correction currently unavailable in commercial EBSD packages. Additionally, extraordinarily long dwell times per pixel would have been required during EBSD to obtain good x-ray statistics, and this would have led to significant, local surface contamination that degrades and even destroys the EBSD patterns.

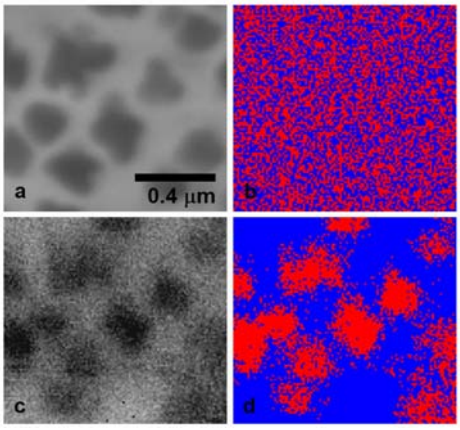

Figure 8. **(a) Backscattered electron micrograph of the region scanned. The initial phase map from the scan shown in (b) illustrates the poor distinguishing ability between the similar g and g' phases. Using the diffraction contrast shown in (c) to distinguish the phases, a significantly better phase map results (d). The slight positional shift of the phases the near the bottom of the EBSD map, seen when comparing (a) with (c-d), was due to sample drift during acquisition.**

Ultimately, the subtle band contrast between the γ and γ' proved to be the most useful feature for distinguishing the phases with EBSD. A one micron square region of the sample was selected for automated EBSD mapping that included several γ' precipitates. Both the γ and γ' phases were selected for mapping, and the band detection settings were

modified to maximize the subtle difference in band contrast. The map step size was 10 nm. As before, direct phase differentiation based on structure was not possible. Figs. 8(a) and (b) shows backscattered image of the region compared to the indexed phase map. The poor correlation is obvious, as the differentiation was essentially random. However, a band contrast map from the same scan, shown in Fig. 8(c), demonstrated the ability of EBSD automated indexing to detect the subtle difference in band contrast between the two phases. By subsequently reassigning the phase of each indexed point based on a threshold value of the band contrast it was possible to improve the phase differentiation dramatically, as shown in Fig. 8(d).

It is important to note that although band contrast thresholding worked well for γ and γ' phase differentiation, it is generally not advisable to distinguish phases using band contrast alone. One reason is that band contrast depends on the phase orientation, since this dictates which Kikuchi bands are present in an EBSD pattern. Consequently, the band contrast difference between two phases may invert for a different set of orientations. This is not a concern in the case discussed, since γ' precipitates coherently with γ. This ensures that within a given parent grain the same Kikuchi bands are present in the EBSD patterns of both phases, so the band contrast is directly comparable.

Case 3: Volume Fraction Determination in a Multiphase Alloy

By their very nature, EBSD datasets rely on statistics to yield information such as texture, misorientation distributions, and grain size. Using EBSD phase identification capabilities, the type of information yielded from datasets can be extended to include phase relations and quantitative distributions. Such a capability is extremely valuable when studying the material behavior of multiphase systems, and this study is an example of employing such an approach with EBSD phase identification.

For this case, we study Alloy 22 (also referred to as C22 in the literature), a Ni-Cr-Mo alloy that possesses one of the highest corrosion

resistance properties of engineering metals. It is primarily specified for use as an outer barrier in long life (>100 year) applications where corrosive environments may exist. Due to its composition, however, Alloy 22 has a propensity for forming intermetallic secondary phases (particularly at high temperatures), usually referred to tetrahedrally close paked (TCP), that are known to decrease its corrosion performance (Hodge and Kirchner 1976, Heubner et al. 1989). Accurate estimations of the degree of secondary phase formation are therefore necessary to forecast the potential decrease in material performance.

The long timescales involved in Alloy 22 applications dictate that phase stability models are required to predict material behavior, and subsequent validation of these models must then rely on characterization of specimens artificially aged at elevated temperatures. Specifically, the extent of the transformed phases as a function of aging condition must be determined in order for direct comparisons to model predictions to be performed.

Research on the possible intermetallics that may form for a multicomponent alloy rich in Ni, Cr, and Mo indicated that a large number can exist. Fortunately, a sufficient amount of previous work was found in the literature that limited the number of potential phases that may precipitate during the aging treatment to three distinct types: σ, P, and μ (Leonard 1969, Raghavan et al 1982, Cieslak et al. 1986). While valuable, this information was insufficient on its own to allow for immediate data collection, and two other pieces of information were needed: are these the same phases present in *our* material, and what method could be used to distinguish between them (*i.e.* composition, crystallography or a combination of both).

To answer these questions, TEM thin sections were made from aged specimens. Three distinct types of secondary phases were observed (Fig. 9), and were determined to be the three TCP phases reported in the

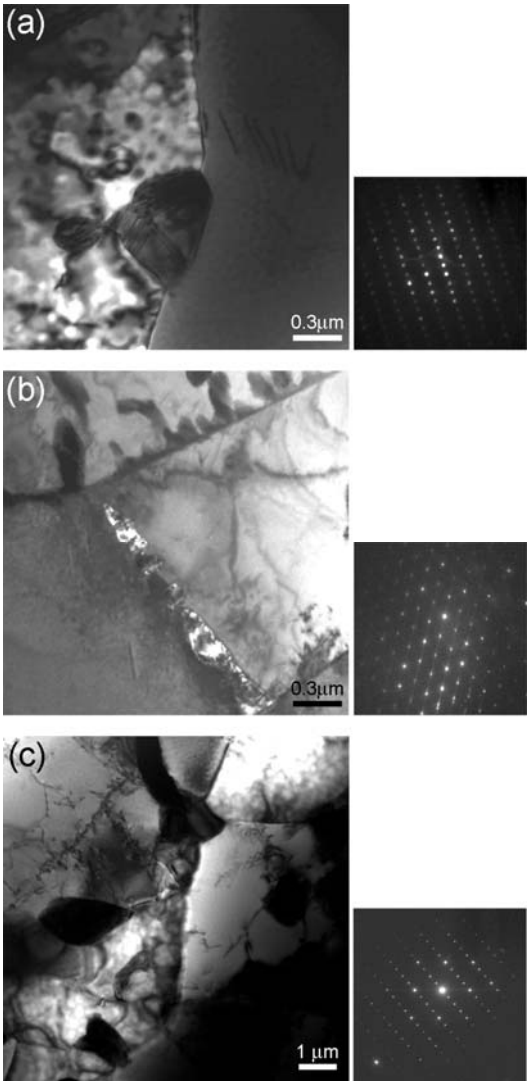

Figure 9. The three types of secondary phases observed in TEM thin sections of aged Alloy 22. These were subsequently identified as (a) μ phase, (b) P phase, and (c) σ phase.

literature by indexing their respective diffraction patterns. Using EDS, compositional differences between the three phases were also measured. While variations existed, these were found to be too small (within 3%) to be useful when performing EDS discrimination on an SEM (due to the larger spot size). Fortunately, the three phases were crystallographically distinct from each other as well as the parent fcc matrix, allowing for direct discrimination between them, and their structures are presented in Fig. 10. Armed with this information, we could now attempt to identify the phases using EBSD.

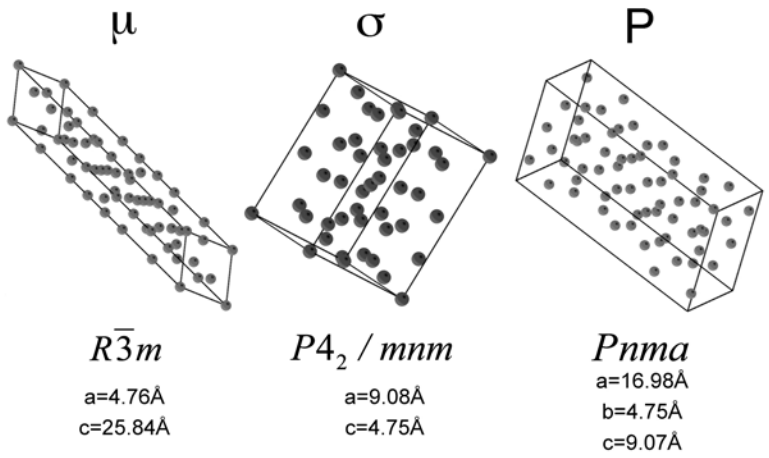

Figure 10. Unit cells and crystal structures of the three TCP phases in aged Alloy 22.

As these phases are atypical, materials files for each needed to be created first (these are the that files contain the information required to calculate the interplanar relations used to index diffraction patterns). The first step to creating these files was looking up the powder diffraction files (PDF) for the prototype compounds for each of the three secondary phases within the International Centre of Diffraction Data (ICDD) database. Within the EBSD data collection software (TSL OIM 4.6 in this case), the crystal structure was defined, and the 25 reflector families (planes families) with the highest intensity reported in the PDFs were entered. While 25 reflector families is a relatively large

number (cubic systems need at most 7), consideration of the lower symmetry of the phases as well as the differences in structure factor between X-ray diffraction and electron diffraction meant that we needed to start by considering an artificially high number of reflectors.

A systematic approach was then needed to whittle the number of reflectors down, and this was begun by manual inspection. Patterns were collected from more than 50 individual secondary phase precipitates as well as from the fcc matrix. The highest resolution possible (non-binned) was used, and the diffraction pattern from the fcc matrix was employed to precisely calibrate the pattern center. As one would expect from three different crystal structures, three distinct types of diffraction patterns were observed as shown in Fig. 11. Since only one TCP structure (μ) possessed a rhombohedral structure, it would be the only one with diffraction patterns with 3-fold symmetry. Restricting the possible phases solely to the μ phase, and iteratively down-selecting the number of reflectors, the pattern was indexed to a fit of better than 0.5°.

To distinguish between the P and σ phases was a greater challenge, and the morphology of the precipitates was used. The TEM observations suggested that the σ phase only formed at grain boundaries, and possessed a more rounded (globular) morphology, whereas the P phase tended to form a more elongated crystal, and not necessarily at the boundaries. By limiting the patterns examined to those obtained from rounded precipitates at grain boundaries and the possible solely to the σ phase, we iterated as we had done previously with the μ phase to down-select the reflectors, again ending with an indexed pattern with a fit better than 0.5°.

Comparison between the μ and σ phase diffraction patterns and the third, as of yet, unindexed pattern type revealed the presence of significantly stronger higher order rings in the μ and σ patterns (Fig. 12), allowing us to then restrict the analysis of the P phase to patterns with either very weak or no rings. Following the same reflector down-selecting procedure as before, the patterns were indexed for the P phase.

Though individual patterns were now successfully indexed, this was accomplished by limiting the possible phases to the single phase during the indexing. During the automated data collection however, all four phases need to be considered as possible solutions for each pattern. To this end, a final fine-tuning of the reflectors list for each phase was performed, ensuring that patterns previously associated with a specific phase were still indexed as that phase despite the possibilities of other phase options.

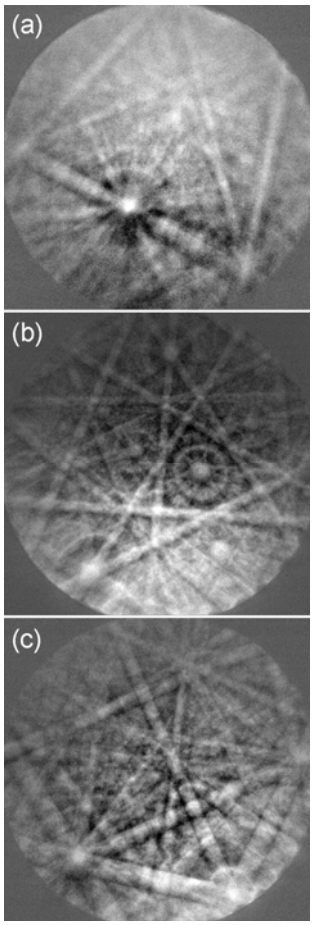

Figure 11. Examples of the three distinct EBSD pattern types obtained from precipitates in aged Alloy 22. These were identified as (a) μ phase, (b) σ phase, and (c) P phase as described in the text.

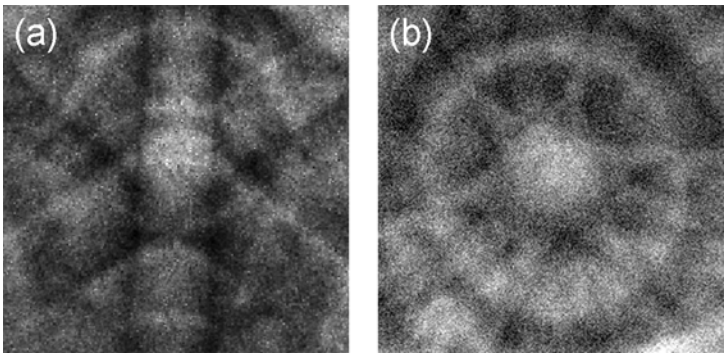

Figure 12. HOLZ rings observed in diffraction patterns from both (a) μ phase and (b) σ phase particles.

Multiple EBSD scans were then performed on five Alloy 22 samples, each aged at a different condition (Table1), and a total of 10^6 data points per sample was collected to ensure a statistical significance to the quantification of the secondary phase content. A limitation of the approach however was immediately apparent when examining the first dataset: some intragranular regions of the scan area that had low image quality (diffraction contrast) were indexed as the matrix (fcc), while others, usually the larger ones, where indexed as the μ phase as seen in Fig. 13. By returning to the area and manually examining the diffraction patterns, it was apparent that these were μ precipitates with sizes less than 0.5μm, and convoluted patterns were being generated form these areas, consisting of both μ phase and fcc diffraction, and subsequently being indexed as fcc.

Table 1. Aging conditions of Alloy 22 samples.

Sample	Temp. (°C)	Time (hours)
A	760	1,000
B	760	2,000
C	760	16,000
D	750	10,076
E	800	1,000

To address this issue, a post-scan processing code was written to assign low image quality points indexed as fcc to the μ phase instead (Fig. 14), similar to that used in *Case 2*. Although no crystallographic information could be assigned to these points, this allowed for an

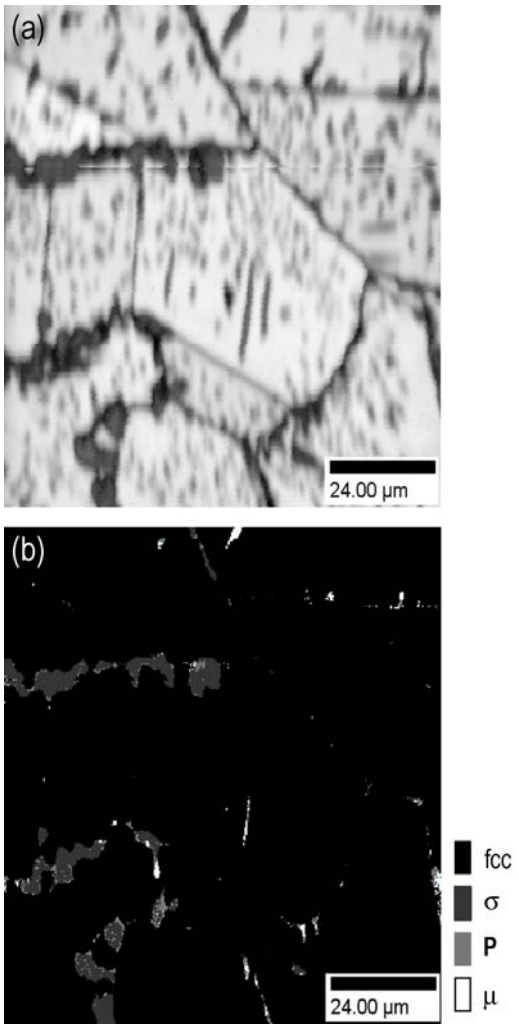

Figure 13. Diffraction contrast map (a) illustrating how only the coarse intragrain μ phase particles are indexable, as shown in (b).

accurate representation of the secondary phase content of the material. It is critical to note that this was possible only because of a combination of excellent polish quality and a well-annealed matrix, as polishing artifacts or defected material regions would also yield low diffraction contrast, rendering this analysis incorrect.

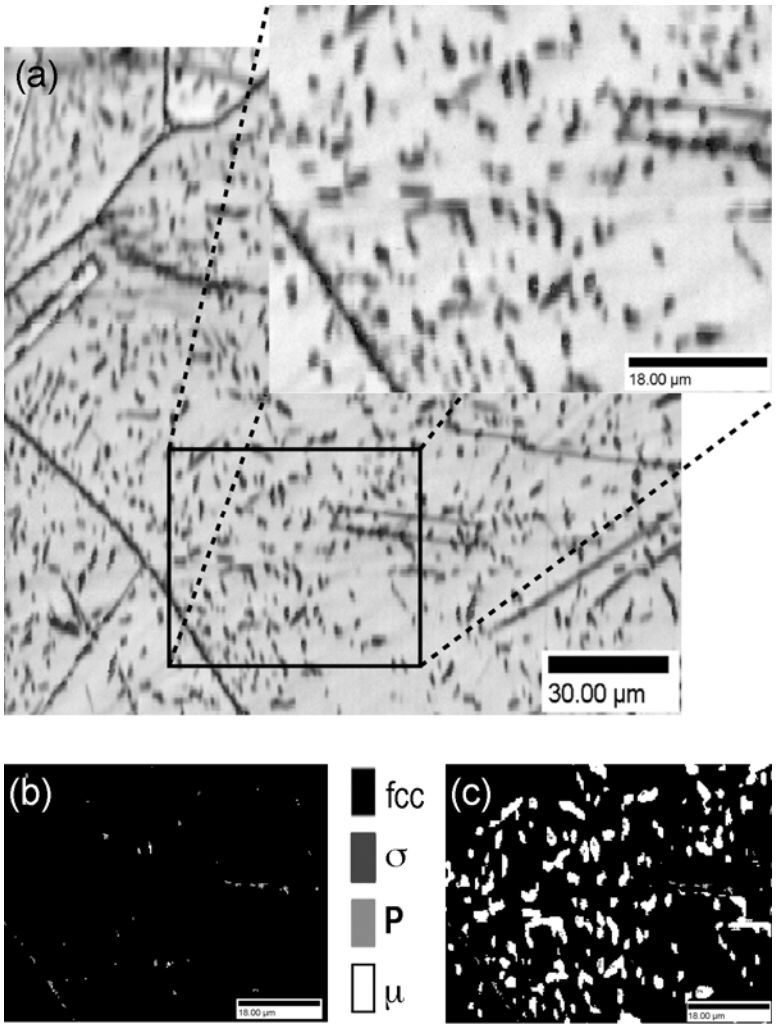

Figure 14. An example of how diffraction contrast is used to correctly adjust the phase information: (a) region of interest, (b) phase map prior to correction, and (c) phase map after correction.

In order to determine whether or not the measurements obtained using this method were accurate, the values were compared to those measured using an image analysis (IA) procedure applied to backscattered electron images captured in the SEM. The IA procedure relies on the contrast difference between the secondary phases and the matrix, such that by applying a threshold to the image the area fraction (and subsequently volume fraction) of all the precipitates can be measured.

Table 2. Phase volume fraction determination using EBSD vs. image analysis.

	Individual Phase Volume Fraction from EBSD			Total Volume Fraction	
Sample	μ	σ	P	EBSD	Image Analysis
A	6.7	0.2	0.1	7.0	6.3
B	9.4	0.2	0.2	9.9	10.1
C	20.2	1.4	0.5	22.1	22.5
D	16.6	0.5	0.6	17.8	17.9
E	11.9	0.3	0.2	12.5	12.7

Comparisons of the total secondary phase volume fraction results using EBSD to those obtained from the IA procedure are shown in Table 2. It can be seen that the total volume fraction measured using EBSD is within 10% of that measured using image analysis, validating the approach. More significant however is the fact that the use of EBSD has yielded the volume fraction of the specific phases present, and not just a total.

ACKNOWLEDGEMENTS

Part of this work was performed under the auspices of the U.S. Department of Energy by Lawrence Livermore National Laboratory in part under Contract W-7405-Eng-48 and in part under Contract DE-AC52-07NA27344.

REFERENCES

Baba-Kishi KZ (1998) Measurement of Crystal Parameters on Backscatter Kikuchi Diffraction Patterns. Scanning 20:117-127

Baba-Kishi KZ (2002) Review: Electron Backscatter Kikuchi Diffraction in the Scanning Electron Microscope for Crystallographic Analyses. J Mat Sci 37:1715-1746

Baba-Kishi KZ, Dingley DJ (1989) Backscatter Kikuchi Diffraction in the SEM for Identification of Crystallographic Point Groups. Scanning 11:305-312

Baba-Kishi KZ, Dingley DJ (1989a) Application of Backscatter Kikuchi Diffraction in the Scanning Electron Microscope to the Study of NiS_2. J Appl Cryst 22:189-200

Cieslak MJ, Headley TJ, Romig AD Jr (1986) The Welding Metallurgy of HASTELLOY Alloys C-4, C-22, and C-276. Met Trans A 17A:2035-2047

Davis JR (ed) (1997) Heat Resistant Materials ASM Specialty Handbook, ASM International, Materials Park

Goehner RP, Michael JR (1996) Phase Identification in a Scanning Electron Microscope Using Backscattered Electron Kikuchi Patterns. J Res Natl Inst Stand Technol 101:301-308

Gourgues-Lorenzon AF (2007) Application of electron backscatter diffraction to the study of phase transformations. Int Mat Rev 52:65-128.

Heubner UL, Altpeter E, Rockel MB et al (1989) Electorchemical Behavior and Its Relation to Composition and Sensitization of NiCrMo Alloys in ASTM G-28 Solution. Corrosion 42:249-259

Hodge FG, Kirchner RW (1976) An Improved Ni-Cr-Mo Alloy for Corrosion Service. Corrosion 32:332-336

Leonard RB (1969) Thermal Stability of Hastelloy Alloy C-276. Corrosion 25:222-228

Michael JR, Eades JA (2000) Use of Reciprocal Lattice Layer Spacing in Electron Backscatter Diffraction Pattern Analysis. Ultramicroscopy 81:67-81

Raghavan M, Berkowitz BJ, Scanlon JC (1982) Electron Microscopic Analysis of Heterogeneous Precipitates in Hastelloy C-276. Met Trans A 13A:979-984

Small JA, Michael JR (2001) Phase Identification of Individual Crystalline Particles by Electron Backscatter Diffraction. J Microscopy 201:59-69